Cobalt sulfide nanoflakes grown on graphite foam for Na-ion batteries with ultrahigh initial coulombic efficiency

Wang, Haisheng; Liu, Jilei; Wang, Huanhuan; Cai, Xiaoyi; Ye, Xinli; Zhang, Lili; Chen, Zhen; Shen, Ze Xiang

2020

Wang, H., Liu, J., Wang, H., Cai, X., Ye, X., Zhang, L., ... Shen, Z. X. (2020). Cobalt sulfide nanoflakes grown on graphite foam for Na-ion batteries with ultrahigh initial coulombic efficiency. Journal of Materials Chemistry A, 8(30), 14900–14907. doi:10.1039/D0TA04312E

https://hdl.handle.net/10356/143875

https://doi.org/10.1039/D0TA04312E

Cobalt Sulfide Nanoflakes Grown on Graphite Foam for Na-Ion Batteries with Ultrahigh Initial Coulombic Efficiency

Haisheng Wang[a], Jilei Liu[d], Huanhuan Wang[a], Xiaoyi Cai[a], Xinli Ye[c,e], Lili Zhang[f], Zhen Chen[b,*] and Ze Xiang Shen[a,c,*]

[a] School of Materials Science and Engineering, Nanyang Technological University, 50 Nanyang Avenue, 639798, Singapore.

[b] Energy Research Institute (ERI@N), Interdisciplinary Graduate School, Nanyang Technological University, 637553, Singapore.

[c] School of Physical and Mathematical Sciences, Nanyang Technological University, 21 Nanyang Link, 637371, Singapore.

[d] College of Materials Science and Engineering, Hunan Province Key Laboratory for Advanced Carbon Materials and Applied Technology, Hunan University, Changsha, 410082, China.

[e] College of Materials Science and Technology, Nanjing University of Aeronautics and Astronautics, 29 Jiangjun Road, 211106, China.

[f] Institute of Chemical Engineering and Science, A* Star, 1 Pesek Road, Jurong Island 627833, Singapore.

Corresponding Authors

[*] E-mail: zchen030@e.ntu.edu.sg (Zhen Chen), zexiang@ntu.edu.sg (Ze Xiang Shen).

Abstract

Sodium-ion batteries (SIBs) are regarded as promising low-cost alternatives to the prevailing lithium-ion batteries. However, most anode materials for SIBs suffer from low initial Coulombic efficiency (ICE), limiting their commercial applications. Herein, we demonstrate a Na-ion anode with an extremely high ICE of 99.4%, based on cobalt sulfide (Co_9S_8/CoS) nanoflakes grown on graphite foam (GF) in diglyme-based electrolyte. The achievement of such a high ICE can be ascribed to the following three aspects: i) negligible side reactions between diglyme-based electrolyte and Co_9S_8/CoS, owing to much higher Fermi level of diglyme reduction than anode potential μ_A of Co_9S_8/CoS, which can block electron transfer from anode to electrolyte, ii) highly reversible conversion reaction of Co_9S_8/CoS, and iii) much lower initial capacity loss of substrate GF, compared with other sorts of carbon. The underlying rules revealed in this study serve as general guidelines in the development of sodium-ion anodes to achieve superb ICE.

Introduction

In recent years, the issues of fossil fuel exhaustion and severe environmental pollution have promoted the rapid development of electric vehicles powered by lithium-ion batteries (LIBs), which, however, will further increase the price of lithium resources.[1-4] In this regard, sodium-ion batteries (SIBs) are very promising alternative candidates for LIBs, owing to the abundance and inexpensiveness of Na resources as well as similar chemical properties between Li and Na.[5-7] Discovering suitable electrode materials for SIBs has become a major challenge for the realization of practical applications.[8, 9]

Various materials have been investigated as sodium-ion anodes, mainly including three types: insertion-type materials (for example, hard carbon and graphite), conversion-type materials (for example, transition metal sulfides and oxides) and alloying-type materials (such as tin and phosphorous).[10-12] Among them, the conversion-type materials have drawn increasing attention owing to their higher specific capacities than those of insertion-type, and smaller volume changes during electrochemical reactions than those of alloying-type.[13] As typical conversion-type materials, cobalt sulfides (i.e., Co_9S_8, CoS, CoS_2) have been widely investigated as Na-ion storage anodes.[14-16] However, the conversion-type anode materials suffer from low energy efficiency owing to the severe voltage decay during charge/discharge process, relative to intercalation-type anode materials.[17-19] The conversion reaction of cobalt sulfides also suffers from sluggish kinetics and severe volume expansion, causing poor rate and cycling performance, respectively.[20-22]

Improved rate capability and cycling stability of cobalt sulfide-based anodes for SIBs have been achieved through coupling various nanosized cobalt sulfides with different carbon materials.[23-25] The Na-ion diffusion length can be shortened due to nanosized cobalt sulfides and fast electron transfer can be accomplished by highly conductive carbon. Furthermore, the strain resulted from

the large volume change of cobalt sulfides can be greatly accommodated by its nanostructures as well as the carbon matrix as a buffer layer.[26] Nevertheless, most of previously reported cobalt sulfide-based anode materials suffered from low initial Coulombic efficiency (ICE), which is less a problem in the case of half cells which usually supply sufficient Na ions from thick metallic Na. However, when assembling full cells, sufficiently high ICE of electrode materials is essential for obtaining high cell performance, because higher ICE can ensure lower irreversible loss of Na ions from the cathodes and lead to higher reversible capacities in full cells.[27-31] However, until now, no effective strategies have been proposed to settle the issue of low ICE for cobalt sulfide-based electrodes.

Herein, we report a strategy of growing CoS_x (Co_9S_8/CoS) nanoflakes on the substrate of graphite foam (GF) through a one-pot solvothermal route (denoted as CoS_x NF@GF hereafter). When coupled with diglyme-based electrolyte, the freestanding CoS_x NF@GF exhibited an ultrahigh ICE of 99.4%. To our knowledge, this is the highest among the previously reported Na-ion storage anodes based on cobalt sulfides. The underlying reasons were uncovered by investigating the following four aspects: electrochemical stability of electrolytes, crystal phase of cobalt sulfides, initial capacity loss of employed carbon, and morphology of cobalt sulfides, where the first three factors were revealed to play the major role in achieving such an extremely high ICE. While the morphology has little influence on the ICE, it nonetheless showed a great impact on the cycling and rate performance, predominantly by alleviating the volume expansion and enhancing the ionic and electronic kinetics in the case of CoS_x ultrathin nanoflakes on GF. Our study provides a deeper understanding of developing anode materials for SIBs with superb ICE.

Results and discussion

Material synthesis and characterization

Figure 1 schematically shows the fabrication procedures of CoS_x NF@GF. In brief, the as-prepared highly conductive and flexible GF was used as the substrate to grow CoS_x (Co_9S_8/CoS) nanoflakes on its surface through a one-step solvothermal route. The crystalline structure and morphology of GF were identified via X-ray diffraction (XRD) and scanning electron microscopy (SEM), respectively, shown in **Figure S1a, b**.

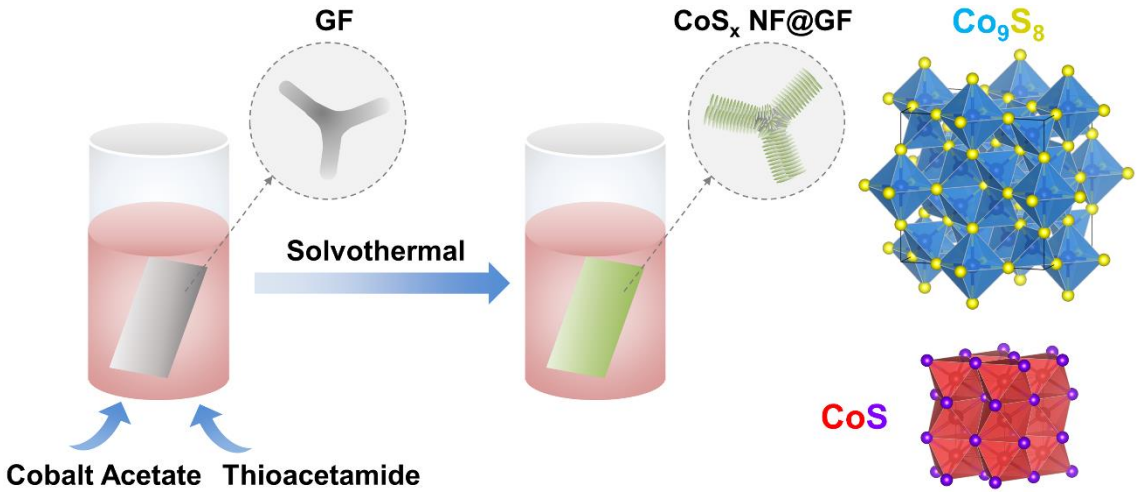

Figure 1. Schematic illustration for synthesis procedures of the CoS_x NF@GF composite and crystal structures of Co_9S_8 and CoS.

The XRD pattern of CoS_x NF@GF is displayed in **Figure 2a**, in which the diffraction peaks could be assigned to the cubic Co_9S_8 (ICDD card no. 04-004-4525) as well as the hexagonal CoS (ICDD card no. 01-075-0605), except for those peaks attributed to GF, demonstrating that the CoS_x composed of Co_9S_8 and CoS phases (the crystal structures shown in **Figure 1**) were grown on GF. In addition, the CoS/Co_9S_8 ratio was estimated to be 0.49 from the XRD pattern using the method of reference intensity ratio. The SEM images (**Figure 2b, c**) display the typical nanoflakes array morphology with a thickness of ~15 nm of CoS_x NF@GF uniformly and vertically aligned on the entire surface of GF. Additionally, the homogenous elemental distribution of Co, S and C within

the sample was validated by the energy-dispersive X-ray spectroscopy (EDS) elemental mappings (**Figure 2d-f**) of the corresponding region shown in **Figure 2c**.

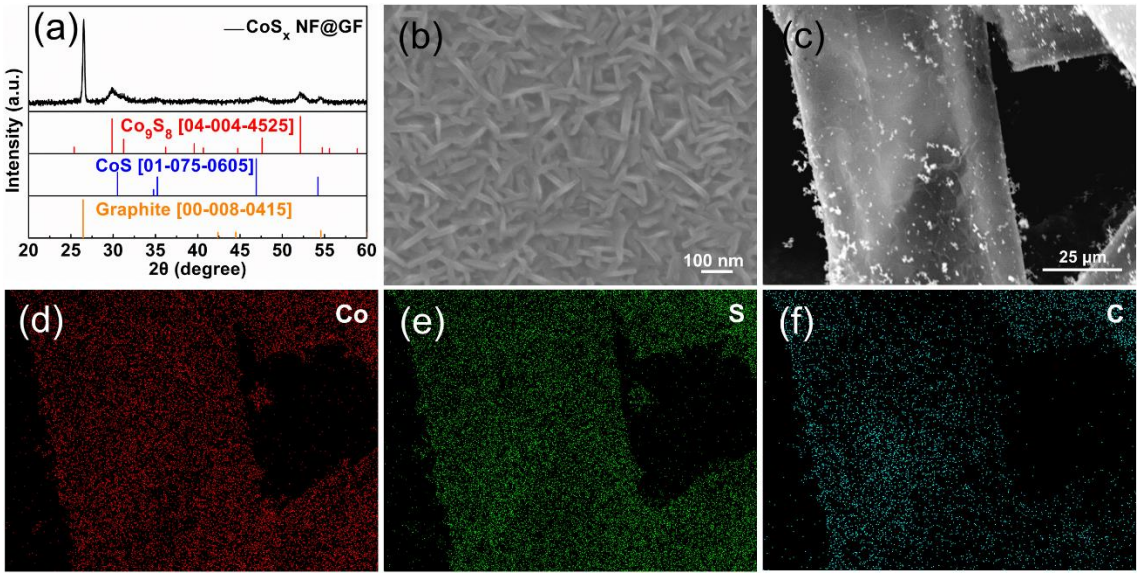

Figure 2. (a) XRD pattern, (b, c) SEM images, (d-f) EDS mappings of Co, S and C elements of the CoS_x NF@GF composite.

The chemical and electronic state of CoS_x NF@GF was analyzed by X-ray photoelectron spectroscopy (XPS). The XPS survey scan spectrum displayed in **Figure 3a** corroborates the existence of Co, S, C, and O four elements in the CoS_x NF@GF composite. The Co 2p core-level XPS spectrum is shown in **Figure 3b**, in which two peaks for Co-S bonds (Co $2p_{3/2}$ and Co $2p_{1/2}$) in cobalt sulfides are observed at 778.8 and 793.9 eV, respectively, with the energy separation of 15.1 eV.[32] Additionally, two corresponding satellite peaks at 781.2 and 797.1 eV can be observed. Another two peaks at 785.6 and 802.6 eV are ascribed to Co-O bonds, because oxygen in the air is easily absorbed on cobalt ions due to their strong affinity.[21, 22, 33] Three types of S components were identified in the high-resolution S 2p spectrum (**Figure 3c**). Two characteristic peaks at 161.9 and 163.1 eV correspond to S $2p_{3/2}$ and S $2p_{1/2}$ of cobalt sulfides (Co-S bonds), respectively, with the energy separation of 1.2 eV.[32] Another two characteristic peaks located at 164.8 and 166 eV

could be attributed to C-S $2p_{3/2}$ and $2p_{1/2}$. Additionally, the remaining two peaks for S-O bonds are located at 167.6 and 168.8 eV, probably due to the oxidation of air. The C 1s core-level XPS spectrum (**Figure 3d**) confirms the presence of C-C, C-S, and C=O bonds with the corresponding peaks centred at 284.6, 286.0 and 288.2 eV, respectively, indicating that S and O-containing groups existed on the surface of GF.[21]

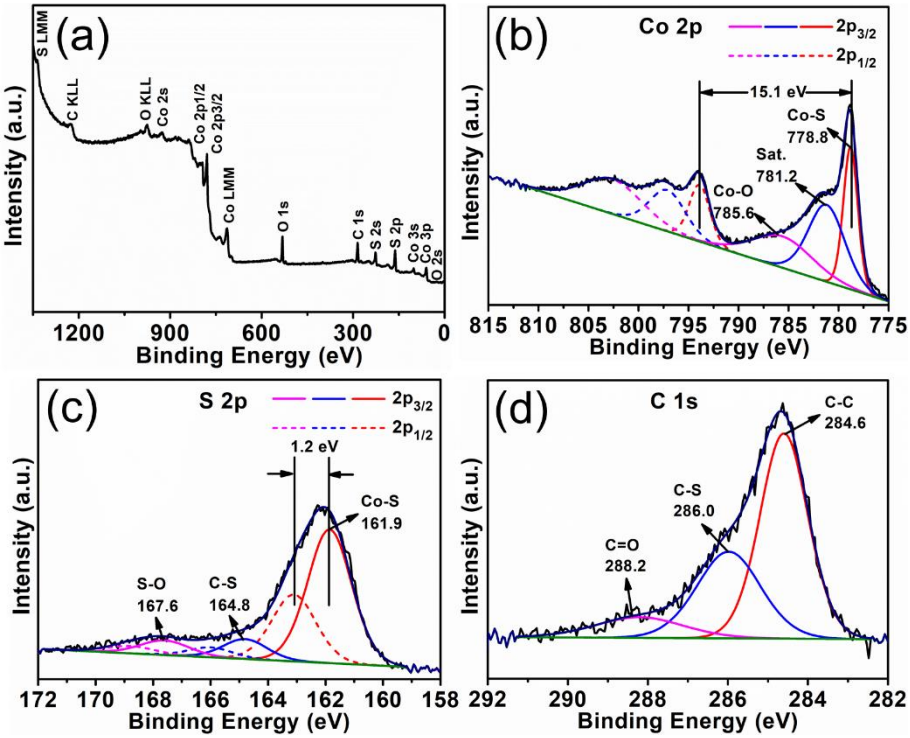

Figure 3. (a) XPS survey scan spectrum, (b) Co 2p, (c) S 2p, and (d) C 1s core-level spectra of CoS_x NF@GF.

Initial Coulombic efficiency

To evaluate the Na-ion storage performance of CoS_x NF@GF, CR2032 half coin cells were assembled with freestanding CoS_x NF@GF as the working electrode and 1 M $NaCF_3SO_3$ in diglyme as the ether-based electrolyte.[34] The discharge/charge profiles of CoS_x NF@GF in diglyme-based electrolyte for the initial three cycles at a current density of 0.5 A g^{-1} between 0.4 and 2.9 V are shown in **Figure 4a**. The long discharge plateau located at ~0.9 V and the long

charge plateau observed at ~1.7 V correspond to the conversion reaction of Co_9S_8/CoS.[21, 22] Additionally, another pair of short plateaus at around 0.6 V (discharging) and 0.7 V (charging) was evidenced, which can be ascribed to the co-intercalation reaction of GF.[35-37] CoS_x NF@GF delivers high initial specific discharge and charge capacities of 577.3 and 573.6 mAh g^{-1}, respectively, calculated using the mass of CoS_x, leading to the highest ICE of 99.4% among the reported cobalt sulfide-based Na-ion anodes. When assembling full cells, the sufficiently high ICE of anode materials is essential for obtaining superior cell performance, because higher ICE can ensure less irreversible loss of Na ions from the cathodes and result in higher reversible capacities in full cells.[27-29]

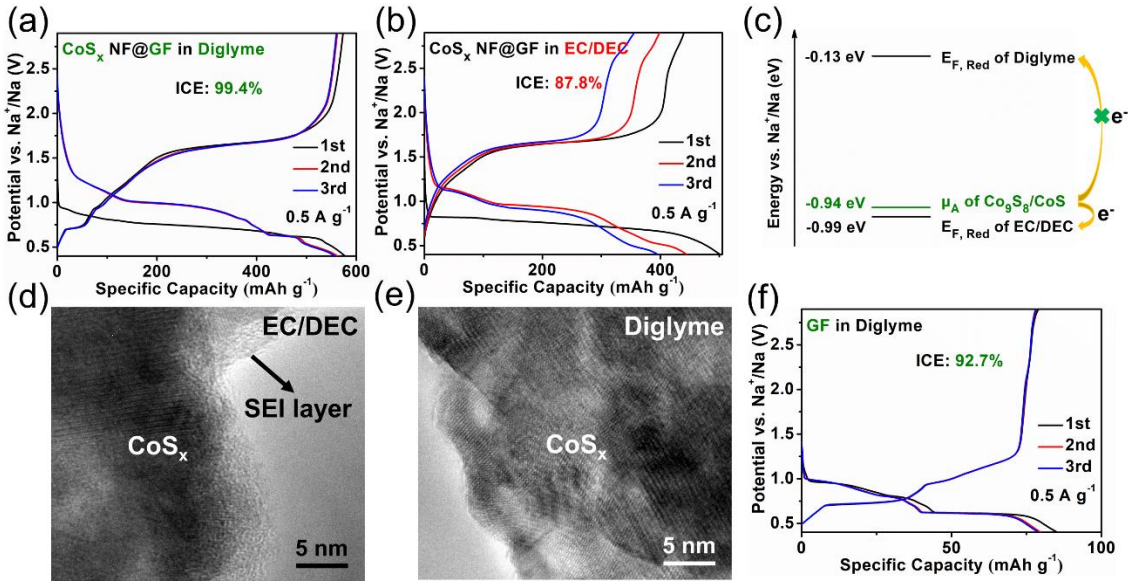

Figure 4. Discharge/charge profiles of CoS_x NF@GF (a) in diglyme-based electrolyte and (b) in EC/DEC-based electrolyte at 0.5 A g^{-1}. (c) Electrochemical stability of diglyme-based and EC/DEC-based electrolytes versus Co_9S_8/CoS electrode. HRTEM images of CoS_x NF@GF electrodes after one cycle (d) in EC/DEC-based electrolyte and (e) in diglyme-based electrolyte. (f) Discharge/charge profiles of pure GF in diglyme-based electrolyte at 0.5 A g^{-1}.

To find out the reasons for such a high ICE for CoS_x NF@GF associated with diglyme-based electrolyte, the impacts of electrolyte and anode material were investigated separately. Firstly, a controlled experiment employing a carbonate-based electrolyte,[38] i.e., 1 M $NaCF_3SO_3$ in ethylene carbonate (EC)/diethyl carbonate (DEC), and CoS_x NF@GF was conducted. With the EC/DEC-based electrolyte, the ICE of CoS_x NF@GF anode was only 87.8%, much lower than that in diglyme-based electrolyte, as demonstrated by the first discharge/charge curves in **Figure 4b**. Furthermore, a drastic capacity decay was observed for the second and third discharge/charge curves, indicating strong irreversible capacity loss resulting from the interactions between CoS_x and EC/DEC-based electrolyte. The underlying reasons are given in **Figure 4c**. The Fermi level of EC/DEC reduction (about -0.99 eV)[39] is lower than the reduction potential μ_A of Co_9S_8/CoS (about -0.94 eV), which means that during the initial sodiation process, electrons can transfer from Co_9S_8/CoS to EC/DEC,[40, 41] leading to electrolyte reduction on the surface of anode, therefore causing initial capacity loss and lower ICE. The solid electrolyte interphase (SEI) layers resulting from EC/DEC reduction were detected by high-resolution transmission electron microscopy (HRTEM) in **Figure 4d**. On the contrary, the Fermi level of diglyme reduction (about -0.13 eV)[39] is much higher than the anode potential μ_A of Co_9S_8/CoS (about -0.94 eV), which can block transfer of electrons from Co_9S_8/CoS to diglyme,[40] resulting in negligible side reactions of electrolyte with anode and thus higher ICE. The HRTEM image (**Figure 4e**) validates no SEI layers formed in diglyme-based electrolyte.

Furthermore, **Table 1** lists some reported anode materials (Co_9S_8, CoS, Ni_3S_2, $Cu_{1.8}S$, ZnSe, and $Co_{0.85}Se$) with verified reversible electrochemical reactions in diglyme-based electrolytes for SIBs.[42-45] The anode potentials μ_A of these materials are all much lower than the Fermi level of diglyme reduction (about -0.13 eV), indicating that no electrons can transfer from anodes to

electrolytes. Actually, after eliminating initial capacity loss from the contributions of employed carbon, all these anode materials exhibit an ICE of nearly 100%, implying negligible side reactions between these anodes and diglyme-based electrolytes. Especially, in the work of $Cu_{1.8}S$ hollow octahedra,[43] the HRTEM measurements revealed that no SEI layers existed at the $Cu_{1.8}S$ surface in diglyme-based electrolyte, but SEI layers were detected in EC/DEC-based electrolyte, originating from side reactions between EC/DEC and $Cu_{1.8}S$.

Table 1. ICE analysis of the reported anode materials in diglyme-based electrolytes for SIBs.

Materials	**Anode Potential μ_A (eV)**	**1st Discharge Capacity (mAh g^{-1}) / ICE (%)**	**1st Discharge Capacity / Initial Capacity Loss of Carbon (mAh g^{-1})**	**Carbon Content (wt%)**	**ICE (%) Calculated without Carbon**	**Ref.**
Co_9S_8/CoS@NSC	-0.9	696/**94.5**	276/116	51	**103.8**	[21]
CoS@rGO	-0.93	780/**89.7**	726/184	41	**99.2**	[22, 46]
(Co_9S_8 QD@HCP)@rGO	-0.9	679/**89.0**	HCP: 415/240 rGO: 375/105	HCP: 6 rGO: 35	**95.6**	[16]
Ni_3S_2@NS-CNTs	-0.9	463/**93.3**	262/43	46	**96.8**	[42]
$Cu_{1.8}S$ Hollow Octahedra	-0.76	403/**99.0**	no carbon	0	**99.0**	[43]
ZnSe NP@NHC	-0.56	311/**99.1**	no data of NHC	6.7	**>99.1**	[44]
$Co_{0.85}Se$ NSs/G	-0.95	470/**82.5**	548/368	21	**98.6**	[45]

The sulfur-poor crystal phases of Co_9S_8 and CoS also contribute to the ultrahigh ICE of CoS_x NF@GF in diglyme-based electrolyte. The conversion reactions of Co_9S_8 and CoS were verified to be highly reversible by ex situ XRD,[21] resulting in negligible initial capacity loss and thus high ICE. From the discharge/charge curves (**Figure 4a**), it is worthwhile to mention that CoS_x NF@GF achieved high reversibility.

Another factor that contributes to the ultrahigh ICE of 99.4% of CoS_x NF@GF in diglyme-based electrolyte is rather low initial capacity loss of substrate GF, resulting from its low capacity (<80 mAh g^{-1}) and high ICE (92.7%), shown in **Figure 4f**. In contrast, other works mostly employed carbon, such as reduced graphene oxide (rGO) or hard carbon, to enhance the electrical conductivity of cobalt sulfide anodes for SIBs.[16, 21, 22] However, as Na-ion storage anodes, rGO, ordered mesoporous carbon (CMK-3) and activated carbon[46] all exhibited substantially higher initial capacity loss with lower ICE in diglyme-based electrolytes, compared with GF, listed in **Table S1.** Thereby, benefiting from the advantageous features of high ICE and low capacity contribution, the selection of GF as the substrate for CoS_x plays also an important role for achieving such an extremely high ICE.

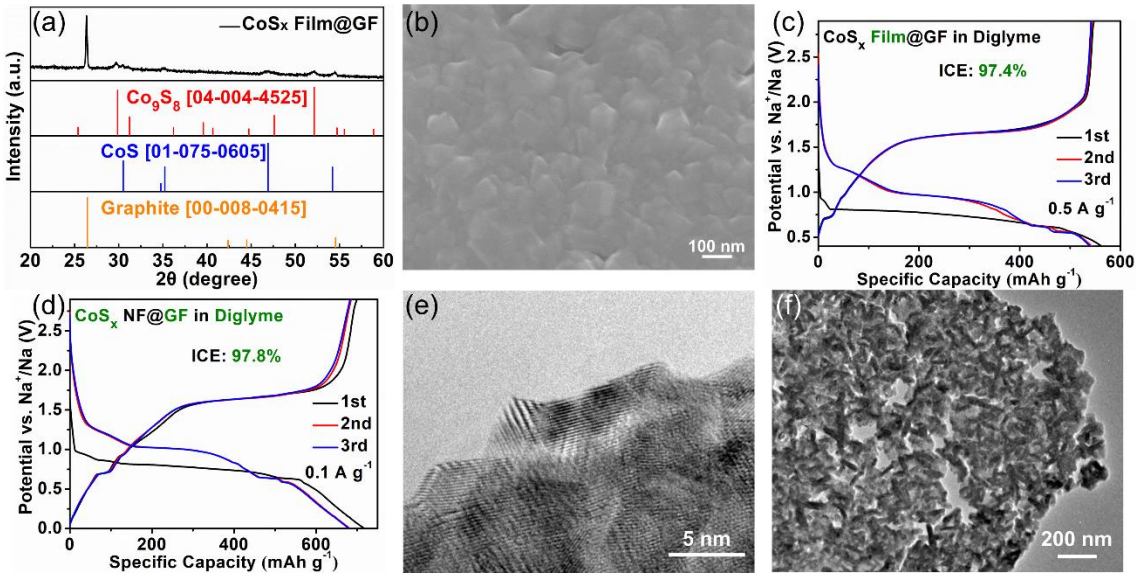

Figure 5. (a) XRD pattern and (b) SEM image of CoS_x Film@GF. (c) Discharge/charge profiles of CoS_x Film@GF in diglyme-based electrolyte at 0.5 A g^{-1}. (d) Discharge/charge profiles of CoS_x NF@GF in diglyme-based electrolyte at 0.1 A g^{-1} in a potential range of 0.01-2.9V. (e, f) HRTEM images of CoS_x NF@GF electrodes after five cycles in diglyme-based electrolyte.

In addition, to investigate the potential impact of morphology of cobalt sulfide on ICE, CoS_x film was grafted on GF via a hydrothermal route, marked as CoS_x Film@GF, which consists of the same phase (Co_9S_8 and CoS) as CoS_x NF@GF, but shows irregular morphology, verified by **Figure 5a, b**. **Figure 5c** shows that the ICE of CoS_x Film@GF in diglyme-based electrolyte was still very high (97.4%), suggesting that the morphology of cobalt sulfide has little influence on ICE.

Furthermore, to explore the potential influence of current density and potential range on ICE, the discharge/charge curves of CoS_x NF@GF in diglyme-based electrolyte were measured at a low current density of 0.1 A g^{-1} in a wide potential range of 0.01-2.9V, shown in **Figure 5d**. The high ICE of 97.8% was still obtained. Additionally, the surface and structure of CoS_x NF@GF electrodes in diglyme-based electrolyte after continuous five cycles were examined by HRTEM. No SEI layers were observed at the surface of electrodes (**Figure 5e**), further verifying highly stable interface between diglyme-based electrolyte and CoS_x. Moreover, most of CoS_x remained the nanoflake structure (**Figure 5f**).

Owing to the three aspects, including the negligible side reactions between diglyme-based electrolyte and Co_9S_8/CoS, the reversible conversion reaction of Co_9S_8/CoS, as well as the rather low initial capacity loss of substrate GF, the CoS_x NF@GF in diglyme-based electrolyte exhibited the highest ICE of 99.4% among the reported cobalt sulfide-based anodes for SIBs, listed in **Table 2**. The lower ICE in other works can be ascribed to carbonate-based electrolytes with side reactions between electrolytes and cobalt sulfides, CoS_2 with irreversible conversion reaction,[15] or employed carbon like rGO, hard carbon with high initial capacity loss.

Table 2. ICE of the previously reported cobalt sulfide-based anode materials for SIBs.

Materials	Cobalt Sulfides	Carbon	Electrolytes	ICE (%)	Ref.
CoS_2/MCNFs	CoS_2	carbonized PAN/PS	1M $NaCF_3SO_3$ in Diglyme	80.2	[14]
CoS_2-C/CNT	CoS_2	carbonized MOFs	1 M $NaPF_6$ in DME	82	[15]
(Co_9S_8 QD@HCP)@rGO	Co_9S_8	rGO, carbonized MOFs	0.5M $NaCF_3SO_3$ in Diglyme	89	[16]
CNT@CoS@C	CoS	CNT, carbonized PDA	1M $NaClO_4$ in EC/DEC with 5 wt% FEC	61	[20]
CoS_x@NSC	Co_9S_8, CoS	carbonized glucose	1M $NaCF_3SO_3$ in Diglyme	94.5	[21]
CoS@rGO	CoS	rGO	1M $NaCF_3SO_3$ in Diglyme	89.7	[22]
CoS⊂carbon NWs	CoS	carbonized glucose	1M $NaClO_4$ in PC with 5 wt% FEC	54	[23]
CoS_2-CoS-GC	CoS, CoS_2	carbonized dextrin	1M $NaClO_4$ in EC/DMC with 5 wt% FEC	68	[24]
Co_9S_8–carbon	Co_9S_8	carbonized PVP	1M $NaClO_4$ in EC/DMC with 5 wt% FEC	68.9	[25]
CoS_x NF@GF	**Co_9S_8, CoS**	**graphite foam**	**1M $NaCF_3SO_3$ in Diglyme**	**99.4**	**This work**

Cycling and rate performance

To investigate electrochemical reactions of CoS_x NF@GF in diglyme-based electrolyte, cyclic voltammetry (CV) measurements were carried out (**Figure 6a**). In the cathodic scans, the three major reduction peaks at 1.22, 0.94 and 0.52 V can be ascribed to the multi-step conversion reactions of Co_9S_8/CoS into Co and Na_2S.[21] In the anodic scans, the two major oxidation peaks at 1.69 and 2.06 V are associated with the reversible formation of Co_9S_8/CoS.[22] Besides, the two main cathodic peaks located at 0.82 and 0.61 V as well as the two main anodic peaks centred at 0.72 and 0.93 V could be attributed to the reversible co-intercalation reactions of substrate GF,[35, 36] which is consistent to the CV curves of pure GF (**Figure S2a**).

Figure 6b compares the cycling performance of three combinations including CoS_x NF@GF in diglyme-based electrolyte, CoS_x Film@GF in diglyme-based electrolyte, as well as CoS_x NF@GF

in EC/DEC-based electrolyte at 0.5 A g^{-1}. It is notable that CoS_x NF@GF in diglyme-based electrolyte delivered not only the highest capacity throughout the entire cycling test, compared to the other two counterparts, but also exhibited the best cycling stability, retaining a high discharge capacity of 491.0 mAh g^{-1} (87.3% of the second-cycle capacity) after 100 cycles. In comparison, the capacity retention of CoS_x Film@GF in diglyme-based electrolyte was lower, i.e., 77.2%. As for CoS_x NF@GF in EC/DEC-based electrolyte, the capacity decreased rapidly to nearly zero at the 20th cycle, an indication of strong irreversible reactions between CoS_x and EC/DEC-based electrolyte. The excellent cycling performance of CoS_x NF@GF in diglyme-based electrolyte can be ascribed to the following two aspects. One is the morphology impact that vertically aligned and ultrathin CoS_x nanoflakes could effectively relieve the strain associated with volume expansion during conversion reactions.[47] The other is the high electrode/electrolyte interfacial stability, owing to negligible side reactions between CoS_x and diglyme-based electrolyte. Additionally, the capacity contribution of GF substrate within CoS_x NF@GF was estimated,[35] shown in **Figure S2b**.

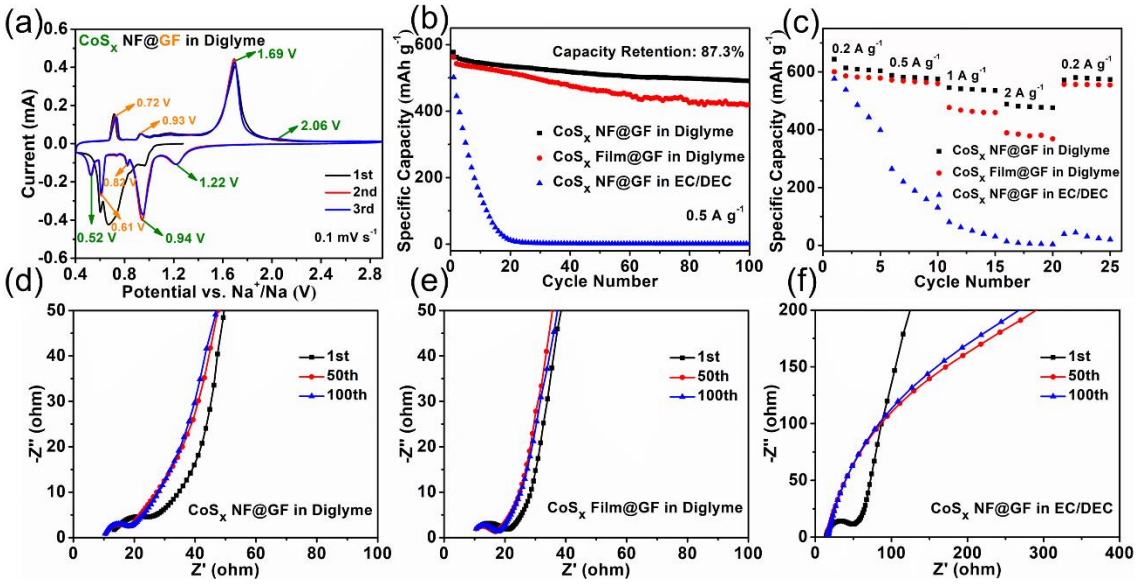

Figure 6. (a) CV curves of CoS_x NF@GF in diglyme-based electrolyte at a scan rate of 0.1 mV s^{-1}. (b) Cycling performance of the three combinations including CoS_x NF@GF in diglyme-based

electrolyte, CoS_x Film@GF in diglyme-based electrolyte, and CoS_x NF@GF in EC/DEC-based electrolyte at 0.5 A g^{-1}. (c) Rate performance of the above three combinations at different current densities from 0.2 to 2 A g^{-1}. (d-f) EIS of the above three combinations at fully charged state after different cycles (1^{st}, 50^{th}, 100^{th}).

Figure 6c exhibits the rate performance of the above three combinations, among which CoS_x NF@GF in diglyme-based electrolyte still showed the best rate capability. In detail, the average discharge capacities were 609, 580, 539, 479 mAh g^{-1} at 0.2, 0.5, 1 and 2 A g^{-1}, respectively. Such excellent rate capability is attributed to the fast Na-ion diffusion deriving from ultrathin CoS_x nanoflakes[48] as well as the small charge-transfer resistance (R_{ct}) at the interface between CoS_x and diglyme-based electrolyte.

To monitor the R_{ct} of the above three combinations, electrochemical impedance spectroscopy (EIS) measurements were conducted after different cycles in **Figure 6d-f**. The R_{ct} can be represented by the diameter of compressed semicircle between high and medium frequency.[21, 49] As for the first cycle, the R_{ct} in diglyme-based electrolyte (**Figure 6d, e**) was substantially smaller than that in EC/DEC-based electrolyte (**Figure 6f**), corresponding to negligible side reactions between diglyme and CoS_x, but existing side reactions between EC/DEC and CoS_x. Moreover, the R_{ct} in diglyme-based electrolyte remained small during cycling, suggesting the highly stable interface between diglyme and CoS_x. In contrast, the R_{ct} in EC/DEC-based electrolyte increased dramatically upon cycling, indicating the very unstable interface between EC/DEC and CoS_x, which is in accordance with the rapid capacity loss for the corresponding cycling performance.

Conclusion

In summary, the CoS_x NF@GF composite has been developed by growing CoS_x (Co_9S_8/CoS) nanoflakes on the highly conductive and flexible substrate of GF through a one-pot solvothermal

route. As a freestanding anode for SIBs, to the best of our knowledge, CoS_x NF@GF in diglyme-based electrolyte achieved the highest ICE of 99.4% among the previously reported cobalt sulfide-based Na-ion anodes. Through a systematic investigation of several factors that can potentially influence the ICE, such a high ICE could be ascribed to the following three aspects, including i) the negligible side reactions between diglyme-based electrolyte and Co_9S_8/CoS, owing to much higher Fermi level of diglyme reduction than anode potential μ_A of Co_9S_8/CoS, blocking transfer of electrons from anode to electrolyte, ii) the highly reversible conversion reaction of Co_9S_8/CoS, and iii) the rather low initial capacity loss of substrate GF. Furthermore, CoS_x NF@GF in diglyme-based electrolyte achieved excellent cycling and rate performance, primarily resulting from alleviated volume expansion and facilitated ionic and electronic kinetics ensured by ultrathin nanoflakes vertically aligned with GF, as well as negligible side reactions at the interface of electrode/electrolyte. These revealed underlying rules can be extended to develop other Na-ion storage anode materials with superb ICE.

Conflicts of interest

There are no conflicts to declare.

Acknowledgements

The authors gratefully acknowledge Ministry of Education (MOE) of Singapore for the funding of this research through the follow grants, AcRF Tier 1 (Reference No: RG103/16); AcRF Tier 1 (RG195/17); AcRF Tier 3 (MOE2016-T3-1-006 (S)).

References

1. Z. Chen, G. T. Kim, D. Bresser, T. Diemant, J. Asenbauer, S. Jeong, M. Copley, R. J. Behm, J. Lin, Z. X. Shen and S. Passerini, *Adv. Energy Mater.*, 2018, **8**, 13.
2. H. Gao, T. F. Zhou, Y. Zheng, Q. Zhang, Y. Q. Liu, J. Chen, H. K. Liu and Z. P. Guo, *Adv. Funct. Mater.*, 2017, **27**, 9.
3. H. L. Pan, Y. S. Hu and L. Q. Chen, *Energy Environ. Sci.*, 2013, **6**, 2338-2360.
4. H. H. Wang, H. S. Wang, S. Chen, B. W. Zhang, G. Yang, P. Gao, J. L. Liu, X. F. Fan, Y. Z.

Huang, J. Y. Lin and Z. X. Shen, *ACS Appl. Energ. Mater.*, 2019, **2**, 7942-7951.
5. G. Q. Zou, H. S. Hou, P. Ge, Z. D. Huang, G. G. Zhao, D. L. Yin and X. B. Ji, *Small*, 2018, **14**, 27.
6. J. L. Liu, Z. Chen, S. Chen, B. W. Zhang, J. Wang, H. H. Wang, B. B. Tian, M. H. Chen, X. F. Fan, Y. Z. Huang, T. C. Sum, J. Y. Lin and Z. X. Shen, *ACS Nano*, 2017, **11**, 6911-6920.
7. J. Liu, C. Xu, Z. Chen, S. Ni and Z. X. Shen, *Green Energy & Environment*, 2018, **3**, 20-41.
8. N. Yabuuchi, K. Kubota, M. Dahbi and S. Komaba, *Chem. Rev.*, 2014, **114**, 11636-11682.
9. S. W. Kim, D. H. Seo, X. H. Ma, G. Ceder and K. Kang, *Adv. Energy Mater.*, 2012, **2**, 710-721.
10. H. Y. Kang, Y. C. Liu, K. Z. Cao, Y. Zhao, L. F. Jiao, Y. J. Wang and H. T. Yuan, *J. Mater. Chem. A*, 2015, **3**, 17899-17913.
11. W. Luo, F. Shen, C. Bommier, H. L. Zhu, X. L. Ji and L. B. Hu, *Accounts Chem. Res.*, 2016, **49**, 231-240.
12. J. Y. Hwang, S. T. Myung and Y. K. Sun, *Chem. Soc. Rev.*, 2017, **46**, 3529-3614.
13. P. Ge, C. Y. Zhang, H. S. Hou, B. K. Wu, L. Zhou, S. J. Li, T. J. Wu, J. G. Hu, L. Q. Mai and X. B. Ji, *Nano Energy*, 2018, **48**, 617-629.
14. Y. L. Pan, X. D. Cheng, L. L. Gong, L. Shi, T. Zhou, Y. R. Deng and H. P. Zhang, *ACS Appl. Mater. Interfaces*, 2018, **10**, 31441-31451.
15. Y. Ma, Y. J. Ma, D. Bresser, Y. C. Ji, D. Geiger, U. Kaiser, C. Streb, A. Varzi and S. Passerini, *ACS Nano*, 2018, **12**, 7220-7231.
16. Z. L. Chen, R. B. Wu, M. Liu, H. Wang, H. B. Xu, Y. H. Guo, Y. Song, F. Fang, X. B. Yu and D. L. Sun, *Adv. Funct. Mater.*, 2017, **27**, 13.
17. W. T. Zheng, P. Lei, D. X. Luo, Y. X. Huang, G. R. Tian and X. D. Xiang, *Solid State Ion.*, 2020, **345**, 6.
18. P. Lei, K. Liu, X. Wan, D. X. Luo and X. D. Xiang, *Chem. Commun.*, 2019, **55**, 509-512.
19. X. Wan, D. X. Luo, P. Lei, Y. X. Huang, X. D. Xiang and M. L. Sun, *Inorg. Chem. Front.*, 2019, **6**, 598-603.
20. F. Han, C. Z. Zhang, B. Sun, W. Tang, J. X. Yang and X. K. Li, *Carbon*, 2017, **118**, 731-742.
21. Q. B. Guo, Y. F. Ma, T. T. Chen, Q. Y. Xia, M. Yang, H. Xia and Y. Yu, *ACS Nano*, 2017, **11**, 12658-12667.
22. S. J. Peng, X. P. Han, L. L. Li, Z. Q. Zhu, F. Y. Cheng, M. Srinivansan, S. Adams and S. Ramakrishna, *Small*, 2016, **12**, 1359-1368.
23. C. Wu, Y. Jiang, P. Kopold, P. A. van Aken, J. Maier and Y. Yu, *Adv. Mater.*, 2016, **28**, 7276-+.
24. J. S. Cho, J. M. Won, J. K. Lee and Y. C. Kang, *Nano Energy*, 2016, **26**, 466-478.
25. Y. N. Ko and Y. C. Kang, *Carbon*, 2015, **94**, 85-90.
26. Z. Hu, Q. N. Liu, S. L. Chou and S. X. Dou, *Adv. Mater.*, 2017, **29**, 24.
27. X. Ou, L. Cao, X. H. Liang, F. H. Zheng, H. S. Zheng, X. F. Yang, J. H. Wang, C. H. Yang and M. L. Liu, *ACS Nano*, 2019, **13**, 3666-3676.
28. X. Zhao, Y. Ding, Q. Xu, X. Yu, Y. Liu and H. Shen, *Adv. Energy Mater.*, 2019, **9**, 10.
29. H. Yang, R. Xu and Y. Yu, *Energy Storage Mater.*, 2019, **22**, 105-112.
30. B. A. Zhang, G. Rousse, D. Foix, R. Dugas, D. A. D. Corte and J. M. Tarascon, *Adv. Mater.*, 2016, **28**, 9824-+.

31. C. C. Wang, L. B. Wang, F. J. Li, F. Y. Cheng and J. Chen, *Adv. Mater.*, 2017, **29**, 7.
32. T. T. Chen, Y. F. Ma, Q. B. Guo, M. Yang and H. Xia, *J. Mater. Chem. A*, 2017, **5**, 3179-3185.
33. F. Han, C. Y. J. Tan and Z. Q. Gao, *J. Power Sources*, 2017, **339**, 41-50.
34. J. Zhang, D. W. Wang, W. Lv, L. Qin, S. Z. Niu, S. W. Zhang, T. F. Cao, F. Y. Kang and Q. H. Yang, *Adv. Energy Mater.*, 2018, **8**, 14.
35. M. Goktas, C. Bolli, E. J. Berg, P. Novak, K. Pollok, F. Langenhorst, M. V. Roeder, O. Lenchuk, D. Mollenhauer and P. Adelhelm, *Adv. Energy Mater.*, 2018, **8**, 11.
36. A. P. Cohn, K. Share, R. Carter, L. Oakes and C. L. Pint, *Nano Lett.*, 2016, **16**, 543-548.
37. B. Jache and P. Adelhelm, *Angew. Chem.-Int. Edit.*, 2014, **53**, 10169-10173.
38. A. Ponrouch, D. Monti, A. Boschin, B. Steen, P. Johansson and M. R. Palacin, *J. Mater. Chem. A*, 2015, **3**, 22-42.
39. A. Ponrouch, E. Marchante, M. Courty, J. M. Tarascon and M. R. Palacin, *Energy Environ. Sci.*, 2012, **5**, 8572-8583.
40. P. Peljo and H. H. Girault, *Energy Environ. Sci.*, 2018, **11**, 2306-2309.
41. J. B. Goodenough and Y. Kim, *Chem. Mat.*, 2010, **22**, 587-603.
42. X. Q. Chang, Y. F. Ma, M. Yang, T. Xing, L. Y. Tang, T. T. Chen, Q. B. Guo, X. H. Zhu, J. Z. Liu and H. Xia, *Energy Storage Mater.*, 2019, **23**, 358-366.
43. H. Park, J. Kwon, H. Choi, D. Shin, T. Song and X. W. D. Lou, *ACS Nano*, 2018, **12**, 2827-2837.
44. Y. Y. He, L. Wang, C. F. Dong, C. C. Li, X. Y. Ding, Y. T. Qian and L. Q. Xu, *Energy Storage Mater.*, 2019, **23**, 35-45.
45. G. J. Zhang, K. H. Liu, S. T. Liu, H. H. Song and J. S. Zhou, *J. Alloy. Compd.*, 2018, **731**, 714-722.
46. J. Zhang, D. W. Wang, W. Lv, S. W. Zhang, Q. H. Liang, D. Q. Zheng, F. Y. Kang and Q. H. Yang, *Energy Environ. Sci.*, 2017, **10**, 370-376.
47. Y. Xu, M. Zhou and Y. Lei, *Adv. Energy Mater.*, 2016, **6**, 24.
48. D. L. Chao, C. R. Zhu, P. H. Yang, X. H. Xia, J. L. Liu, J. Wang, X. F. Fan, S. V. Savilov, J. Y. Lin, H. J. Fan and Z. X. Shen, *Nat. Commun.*, 2016, **7**, 8.
49. K. K. Li, J. Zhang, D. M. Lin, D. W. Wang, B. H. Li, W. Lv, S. Sun, Y. B. He, F. Y. Kang, Q. H. Yang, L. M. Zhou and T. Y. Zhang, *Nat. Commun.*, 2019, **10**, 10.